INTERNATIONAL JOURNAL OF
NUMERICAL ANALYSIS AND MODELING
Volume 13, Number 6, Pages 986–1002

EFFICIENT FINITE DIFFERENCE METHODS FOR ACOUSTIC SCATTERING FROM CIRCULAR CYLINDRICAL OBSTACLE

RUI GUO[1,3], KUN WANG[1,2,*] AND LIWEI XU [1,2]

Abstract. We consider efficient finite difference methods for solving the three-dimensional (3D) acoustic scattering by an impenetrable circular cylindrical obstacle. By using the separation of variable and other techniques, we first transform the 3D problem into a series of one-dimensional (1D) problems in this paper, and then construct some efficient and accuracy finite difference methods to solve these 1D problems instead of the 3D one. There are mainly two advantages for these methods: one is that they are pollution free for the problem to be considered in this paper; and the other is that the linear systems generated from these schemes have tri-diagonal structures. These features lead to easy implementation and much less computational cost. Numerical examples are presented to verify the efficiency and accuracy of the numerical methods, even with the wave number greater than 100.

Key words. Helmholtz equation, circular cylindrical coordinate, finite difference method, pollution free, 3D ocean waveguide.

1. Introduction

In this work, we investigate the 3D acoustic scattering by an impenetrable circular cylindrical obstacle in a 3D shallow ocean waveguide. The shallow ocean waveguide considered here is in an open domain of homogeneous medium between two horizontal boundaries, and the sea surface is pressure release and the sea floor is rigid. This problem can be formulated by the Helmholtz equation with appropriate boundary conditions.

In the past decades, a large number of analytical methods have been developed to deal with the solution of acoustic propagation problems in ocean environments in (see [1, 2, 3, 4, 5, 6, 8, 11, 17, 32] and references therein). Contrary to the analytical methods, we are concerned with efficient and accurate numerical methods for the scattering problem. Many classical numerical methods have been used to solve this problem, such as, finite difference methods [12, 18, 29, 30, 34], boundary integral equation methods [9], finite element methods [14, 15, 20, 21, 26] and spectral methods [24]. In [9], the boundary integral equation method is used to compute the scattered field from the 3D bathymetry in an ocean waveguide. They solve a sequence of 1D integral equations instead of a very large two-dimensional (2D) one because of the azimuthal symmetry. This method is suitable for low-frequency, compact deformation scattering problems where the required number of discrete range steps and azimuthal components are not large. Finite element method is popular to simulate the acoustic scattering (see [15] and references therein). However, the feasible finite element method appears only for low and intermediate frequencies. Pan et al. [20] considered a coupled finite element and DtN mapping method to solve the acoustic scattering problem with an infinite long rectangle cylinder in an

Received by the editors October 18, 2015, and, in revised form June 16, 2016.
2000 *Mathematics Subject Classification.* 65N06, 65N22.

* Corresponding author. This research is supported by the NSFC Grant(11371385, 11201506, 61465011), the start-up fund of Youth 1000 plan of China and that of Youth 100 plan of Chongqing university, and Fundamental Research Funds for the Central universities with project NO. CDJZR14105501 and 106112015CDJXY100007.

oceanic waveguide. The results show that the proposed method is valid and very fast. However, the maximum value of kL tested there is 6.5, with k and L being the wave number and the width of the infinite long rectangle cylinder, respectively. This means that the wave number is quite small. A super-spectral finite element method was developed for the acoustical wave propagation in nonuniform waveguides in [21]. This method is based on a finite-element approach using a mixture of high order shape functions and wave solutions. The computational cost has been drastically reduced.

Although lots of work have been done, an indisputable fact is that huge computational cost is required for the higher dimensional problem. The solution of this problem is highly oscillatory with large wave numbers and the "pollution effect" (see [15]) exists in almost all of these methods.

On the other hand, the finite difference method is also a popular and powerful computational technique for simulating the wave propagation modeling for its easy implementation and computational efficiency [35]. Furthermore, it can be easily extended to the 3D case. Recently, a novel kind of finite difference methods is proposed by Wang et al. to solve the 2D and 3D Helmholtz equations with large wave numbers in the polar and spherical coordinates (see [30]). The main idea of the method is to use the separation of variables and variable transformation to reduce the higher dimensional Helmholtz equation on a special domain into a sequence of 1D equations, and then construct pollution free schemes for approximating the 1D problems. The idea is extend to solving the singularly perturbed equations in [12].

In this paper, we will extend the method proposed in [30] and construct a more accurate finite difference scheme to solve 3D the waveguide problem in the circular cylindrical coordinate. Including applying the algorithms proposed in [30], we also construct a more accurate scheme to simulate the problem. The motivations are as follows: First, due to the circular cylindrical obstacles geometry, via the circular cylindrical coordinate transformation and separation of variables, we can transform the 3D problem into a series of 1D problems similar to [30]. Second, in realistic environments, usually, the magnitude of ocean waveguide depth is less than $10^3 m$, the frequencies are no more than $1000hz$, and the sound velocity is commonly $1500m/s$ in ocean waveguide, indicating that the non-dimensional wave number k is less than 1. However, in the numerical experiment, by scale shift, the magnitude of ocean waveguide depth is less than 10, and correspondingly, the wave number k is probably 100. This will result a huge linear system if solving in 3D directly because of the "pollution effect". Finally, to the best of our knowledge, most of the works are focused on the problems in 2D (range and depth) or 3D without considering azimuth.

The rest of the paper is organized as follows. In Section 2 we transform the 3D problem to a series of 1D problems and introduce the spectral normal mode solution in the circular cylindrical coordinate. Then, we construct the new finite difference schemes to solve the 1D problem in Section 3. In Section 4 we examine the performance of the scheme by testing a series of numerical experiments. Conclusions are presented in Section 5.

2. Ocean waveguide in 3D

We consider the waveguide in an open domain $\Omega \subset \mathbb{R}^3$ full of homogeneous medium between the two horizontal boundaries $z = 0$ (called 'top') and $z = H$ (called 'bottom'), where the sea surface $z = 0$ is pressure release (such as air), the sea floor $z = H$ is rigid (such as rock), and a sound soft of the immersed circular cylindrical obstacle Ω_1 is embedded in Ω, the linear acoustic scattering problem in homogeneous shallow ocean can be described as the Helmholtz equation [3]:

$$\Delta u^s + k^2 u^s = 0, \text{ in } \Omega \setminus \Omega_1, \tag{1}$$

$$u^s \mid_{z=0} = 0, \ \frac{\partial u^s}{\partial z} \mid_{z=H} = 0, \tag{2}$$

$$u^s \mid_{\partial\Omega_1} = -u^i, \tag{3}$$

$$\lim_{r \longrightarrow \infty} \sqrt{r}\left(\frac{\partial u^s}{\partial r} - ik_n u^s\right) = 0, \tag{4}$$

where k is the wave number, and u^i, u^s and u denote the incident, scattered and total fields satisfying ($u = u^i + u^s$), k_n is the nth model horizontal wave number (see Section 2.1), $r = \sqrt{x^2 + y^2}$ and $i^2 = -1$.

2.1. Dimension reduction in the circular cylindrical coordinate. We consider the dimension reduction for the form of the problem (1)–(4) in the circular cylindrical coordinate. Setting

$$x = r\cos(\theta), \ y = r\sin(\theta), \ z = z, \tag{5}$$

we could write (1) in the form

$$\frac{1}{r}\frac{\partial}{\partial r}\left(r\frac{\partial u^s}{\partial r}\right) + \frac{1}{r^2}\frac{\partial^2 u^s}{\partial \theta^2} + \frac{\partial^2 u^s}{\partial z^2} + k^2 u^s = 0. \tag{6}$$

It is known that, applying the method of separation of variables, the scattered field u^s takes the form

$$u^s = \sum_{n=0}^{+\infty} u_n^s(r,\theta)\omega_n(z). \tag{7}$$

where

$$\omega_n(z) = \sqrt{\frac{2}{H}}\sin\left(\left(n + \frac{1}{2}\right)\frac{\pi z}{H}\right), \ n = 0, 1, 2, \cdots, \tag{8}$$

which constitute an orthogonal basis in $L^2(0, H)$.

Substituting (7) into (6), we obtain a series of 2D equations

$$\frac{1}{r}\frac{\partial}{\partial r}\left(r\frac{\partial u_n^s}{\partial r}\right) + \frac{1}{r^2}\frac{\partial^2 u_n^s}{\partial \theta^2} + k_n^2 u_n^s = 0, \ n = 0, 1, 2, \cdots, \tag{9}$$

with the Sommerfeld condition

$$\lim_{r \longrightarrow \infty} \sqrt{r}\left(\frac{\partial u_n^s}{\partial r} - ik_n u_n^s\right) = 0, \tag{10}$$

where $k_n = \sqrt{k^2 - ((n + \frac{1}{2})\frac{\pi}{H})^2}$.

Furthermore, expanding $\{u_n^s\}_{n=0}^{+\infty}$ into Fourier series, we obtain

$$u_n^s = \sum_{m=-\infty}^{+\infty} u_{mn}^s(r)\psi_m(\theta), \tag{11}$$

where

$$\psi_m(\theta) = \frac{1}{\sqrt{2\pi}}e^{im\theta}, m = 0, \pm 1, \pm 2, \cdots, \tag{12}$$

satisfying

$$(\psi_m, \psi_{m'}) = \int_0^{2\pi} \psi_m(\theta)\overline{\psi_{m'}(\theta)}d\theta = \begin{cases} 1, & m = m', \\ 0, & m \neq m'. \end{cases}$$

Substituting (11) into (9), we get a series of 1D equations as follows:

$$\frac{1}{r}\frac{\partial}{\partial r}(r\frac{\partial u^s_{mn}}{\partial r}) + k^2_{mn}u^s_{mn} = 0,\ n = 0, 1, 2, \cdots, m = 0, \pm 1, \pm 2, \cdots, \tag{13}$$

with the Sommerfeld boundary condition, accordingly,

$$\lim_{r\longrightarrow\infty} \sqrt{r}(\frac{\partial u^s_{mn}}{\partial r} - ik_n u^s_{mn}) = 0, \tag{14}$$

where $k_{mn} = \sqrt{k_n^2 - \frac{m^2}{r^2}}$.

Therefore, using the separation of variables, the solution of the problem (1)–(4) in circular cylindrical coordinates has the following form:

$$u^s = \sum_{n=0}^{+\infty}\sum_{m=-\infty}^{+\infty} u^s_{mn}(r)\psi_m(\theta)\omega_n(z),\ \text{in } \Omega \setminus \Omega_1. \tag{15}$$

Suppose

$$\Omega_1 = \{0 < r \leq a; z \in [0, H], \theta \in [0, 2\pi)\},$$
$$\Omega_2 = \{a \leq r \leq b; z \in [0, H], \theta \in [0, 2\pi)\},$$

with $a < b$ being the radius of circular cylindrical obstacles. Applying the DtN operator, we can transform the equation (1) from a unbounded domain $\Omega \setminus \Omega_1$ to a bounded domain $\Omega_2 \setminus \Omega_1$ with the radiation boundary as follows: $\frac{\partial u^s_{mn}}{\partial r} - ik_n u^s_{mn} = g_{2mn}$ with g_{2mn} being a given function.

Through the above process, the 3D problem (1)–(4) in a homogeneous shallow ocean waveguide is transformed to a series of 1D problems as follows:

$$\frac{1}{r}\frac{\partial}{\partial r}(r\frac{\partial u^s_{mn}}{\partial r}) + k^2_{mn}u^s_{mn} = 0\ r \in (a, b), \tag{16}$$

$$u^s_{mn}\mid_{r=a} = g_{1mn}, \tag{17}$$

$$\partial_r u^s_{mn} - ik_n u^s_{mn}\mid_{r=b} = g_{2mn}. \tag{18}$$

For brevity, we let v to denote v_{mn}, and likewise for k_{mn}, g_{1mn} and g_{2mn} in the following. Setting

$$u^s_{mn}(r) = r^{-\frac{1}{2}}v(r), \tag{19}$$

we have

$$-v^{(2)} - k^2(r)v = 0\ r \in (a, b), \tag{20}$$

$$v(r)\mid_{r=a} = a^{\frac{1}{2}}g_1, \tag{21}$$

$$(v^{(1)} - (ik_n + \frac{1}{2r})v)\mid_{r=b} = b^{\frac{1}{2}}g_2, \tag{22}$$

where

$$k^2(r) = k^2 - ((n + \frac{1}{2})\frac{\pi}{H})^2 - \frac{4d_m - 1}{4r^2},\ d_m = m^2(m = 0, \pm 1, \pm 2\cdots). \tag{23}$$

(20) has the same form as the Helmholtz equation, but with a variable wave number $k(r)$, it is possible to apply efficient and accurate numerical methods developed for the Helmholtz equation to solve this problem. Before proceeding, we recall the following result (see [24]):

Lemma 2.1. *Suppose that v is the solution of the problem* (20)-(22), $\|g_1\|, \|g_2\| \leq M_1$ *in the domain* (a, b), *then we have the following stability estimates*

$$\| v \| \leq M_1 \frac{1}{k}, \tag{24}$$

$$\| v^{(1)} \| \leq M_1, \tag{25}$$

$$\| v^{(2)} \| \leq M_1 k, \tag{26}$$

where $\| \cdot \|$ denotes the L^2-norm, M_1 is a general positive constant independent of $k, v, v^{(n)}$, but it depends on g_1, g_2 and the domain, and may take different values at different occurrences.

Remark 2.1. *When we compute* (15), *the convergence of the double-series must be considered. It is shown that the summation of m is taken from* 0 *to M with $M = O(k)$ (see* [15]*), and the summation of n is taken from* 0 *to N, with $N = int[k\frac{H}{\pi} + \frac{1}{2}] = O(k)$(see Section 2.2), hence for problems with large wave number k, it holds $d_m = O(k^2)$. Assuming that the radius of the circular cylindrical obstacle satisfies $a >> h$ and considering the definition of* (23), *we could easily verify*

$$\|(k^2(r))^{(l)}\| = O(k^2), \ l \in Z, \tag{27}$$

which is consistent with the similar result in [30].

2.2. Spectral normal mode solution. In this subsection, we consider the spectral normal mode solution of the problem (1)–(4), which will be used to validate the efficiency of new finite difference methods in the next section.

In fact, for a shallow ocean waveguide with a finite depth, considering the depth-dependent eigenvectors $\omega_n(z)$ in the vertical direction and fourier series in the horizontal direction, the spectral normal mode solution of the problem (1)–(4) has the following representation (see [3, 17])

$$u^s = \sum_{n=0}^{+\infty} \sum_{m=-\infty}^{+\infty} (a_{mn} H_m^{(1)}(k_n r) + b_{mn} H_m^{(2)}(k_n r)) \psi_m(\theta) \omega_n(z), \ \text{in } \Omega_2 \setminus \Omega_1, \tag{28}$$

where $H_m^{(1)}, H_m^{(2)}$ are the m-th degree Hankel functions of the first and second kind, respectively. Assuming that only the outgoing or evanescent contributing modes in the expansion of u^s are physically acceptable, which will be considered as Sommerfeld conditions, it follows that all of the coefficients b_{mn} vanish. Let $N = int[kH/\pi + \frac{1}{2}]$ be the total number of modal (propagating modes), so the modes for $n \in [0, N-1]$ with $\Im(k_n) = 0$ corresponding to the propagating waves, while for $n \geq N$ with $\Re(k_n) = 0$ corresponding to the evanescent wave. Here, $\Im(k_n)$ and $\Re(k_n)$ denote imaginary part and real part of k_n, respectively.

Ignoring the evanescent wave, it yields the scattering solution of the problem (1)–(4) with the following representation

$$u^s = \sum_{n=0}^{N-1} \sum_{m=-\infty}^{+\infty} a_{mn} H_m^{(1)}(k_n r) \psi_m(\theta) \omega_n(z), \ \text{in } \Omega_2 \setminus \Omega_1. \tag{29}$$

On the other hand, assuming that the monochromatic harmonic incident wave u^i is located at the depth z_0 with the moving direction $\theta^{'}$, we have

$$\begin{aligned} u^i &= \sum_{n=0}^{N-1} \omega_n(z)\omega_n(z_0)e^{ik_n(x\cos(\theta^{'})+y\sin(\theta^{'}))} \\ &= \sum_{n=0}^{N-1} \omega_n(z)\omega_n(z_0)e^{ik_n(r\cos(\theta)\cos(\theta^{'})+r\sin(\theta)\sin(\theta^{'}))} \\ &= \sum_{n=0}^{N-1} \omega_n(z)\omega_n(z_0)e^{ik_n r\cos(\theta-\theta^{'})}. \end{aligned} \tag{30}$$

Applying Jacobi-Anger expansion (see [7]), we further obtain

$$u^i = \sum_{n=0}^{N-1} \sum_{m=-\infty}^{+\infty} \omega_n(z)\omega_n(z_0)i^m J_m(k_n r)e^{im(\theta-\theta^{'})}, \tag{31}$$

where J_m is the m-th degree Bessel function of the first kind.

Multiplying (3) by $\psi_m(\theta)\omega_n(z)$, using (29) and (31), and integrating with respect to z, θ from 0 to H and 0 to 2π, we get

$$a_{mn}H_m^{(1)}(k_n r)|_{r=a} = -\sqrt{2\pi}i^m\omega_n(z_0)J_m(k_n r)e^{-im\theta^{'}}|_{r=a},$$

it follows by

$$a_{mn} = -\frac{\sqrt{2\pi}i^m\omega_n(z_0)J_m(k_n a)}{H_m^{(1)}(k_n a)}e^{-im\theta'}.$$

Due to $J_{-m} = (-1)^m J_m$, $H_{-m}^{(1)} = (-1)^m H_m^{(1)}$, when m is a negative integer, there holds

$$a_{-mn} = -\frac{\sqrt{2\pi}i^{-m}\omega_n(z_0)(-1)^m J_m(k_n a)}{H_m^{(1)}(k_n a)}e^{im\theta'}.$$

Therefore, the solution of (1)–(4) in the circular cylindrical coordinate satisfies

$$\begin{aligned} u^s &= \sum_{n=0}^{N-1} \sum_{m=-\infty}^{+\infty} a_{mn}H_m^{(1)}(k_n r)\psi_m(\theta)\omega_n(z), \\ &= \sum_{n=0}^{N-1} \{\frac{a_{0n}}{\sqrt{2\pi}}H_0^{(1)}(k_n r) + \sum_{m=1}^{+\infty}[a_{mn}H_m^{(1)}(k_n r)\psi_m(\theta) \\ &\quad + a_{-mn}H_{-m}^{(1)}(k_n r)\psi_{-m}(\theta)]\}\omega_n(z) \\ &= \sum_{n=0}^{N-1} \sum_{m=0}^{+\infty} c_{mn}H_m^{(1)}(k_n r)\omega_n(z)\cos(m(\theta-\theta^{'})), \end{aligned} \tag{32}$$

where

$$c_{mn} = \begin{cases} \frac{-\omega_n(z_0)J_0(k_n a)}{H_0^{(1)}(k_n a)}, & m = 0, \\ \frac{-2i^m\omega_n(z_0)J_m(k_n a)}{H_m^{(1)}(k_n a)}, & m \in Z^+. \end{cases}$$

3. New finite difference methods

In the above section, by applying the dimension reduction in the circular cylindrical coordinate, we transform the 3D problem into a series of 1D ones, and greatly reduce the computational size. In this section, we will consider some pollution free numerical methods to approximate the reduced 1D problems, which will make further efforts to decrease the computational cost. In [30], Wang et al. proposed several new finite difference schemes for the Helmholtz equation in the annulus and hollow sphere domains under the assumption of

$$kh = C, \tag{33}$$

where C is a general positive constant (even much larger than 1), which means $h = \frac{C}{k}$. The main idea of the new finite difference schemes is based on the Helmholtz equation itself and Taylor expansion. The most significant virtue of the developed difference schemes is that they are pollution free, therefore their convergence orders are independent of the wave number k. Moreover, these schemes are simple and have tri-diagonal structures, which is as simple as the standard second-order difference scheme. The new finite difference schemes are described briefly as follows. The reader is referred to [30] for more details.

Let $0 < h < 1$ be an uniform mesh size satisfying $h = \frac{b-a}{P}$ with $P \in Z^+$, $r_i = a + ih$ $(i \in Z^+, 0 < i \leq P)$. For simplicity, we set $k_i = k(r_i), v_i = v(r_i), v_{i+1} = v(r_i + h)$ and $v_{i-1} = v(r_i - h)$. By Taylor expansion, it is straightforward to show that

$$v_{i+1} + v_{i-1} = 2\Big[v_i + \frac{h^2}{2!}v_i^{(2)} + \frac{h^4}{4!}v_i^{(4)} + \frac{h^6}{6!}v_i^{(6)} + \cdots + \frac{h^{2s}}{(2s)!}v_i^{(2s)} + \cdots\Big]. \tag{34}$$

Instead of using an approach based on a truncated Taylor expansion such as the standard second-order finite difference scheme (SFD) and fourth-order compact finite difference scheme (CFD), the new finite difference schemes take account of the contribution of all even-order derivative terms in the Taylor expansion (34). It shows that by satisfying the original Helmholtz equation, we can know recursively that all terms of even-order derivatives $v_i^{(2s)} (s = 1, 2, 3, \cdots)$ are only determined by $v_i, v_i^{(1)}$. Under the assumption of (33), combining (27) and Lemma 2.1, (34) was rewritten as

$$v_{i+1} + v_{i-1} = 2[D_1 v_i + D_2 v_i^{(1)} + D_{31} v_3 + \cdots], \tag{35}$$

where the grouping of $D_1 v_i, D_2 v_i^{(1)}, D_{31} v_i, \cdots$ depend only on the mesh size h and are independent of the wave number k. Furthermore, they satisfy

$$\|D_1 v_i\| = O(h),\ \|D_2 v_i^{(1)}\| = O(h^2),\ \|D_{31} v_i\| = O(h^3),$$

where

$$D_1 = \cos(k_i h), \tag{36}$$

$$D_2 = \frac{[\frac{1}{4}k_i^2 h^2 \cos(k_i h) - \frac{1}{4}k_i h \sin(k_i h)](k_i^2)^{(1)}}{k_i^4}, \tag{37}$$

$$D_{31} = \frac{[-\frac{1}{12}k_i^3 h^3 \sin(k_i h) - \frac{1}{8}k_i^2 h^2 \cos(k_i h) + \frac{1}{8}k_i h \sin(k_i h)](k_i^2)^{(2)}}{k_i^4}. \tag{38}$$

Therefore, the relationship for the interior points are followed, with different truncation errors, by

$$v_{i+1} + v_{i-1} = 2D_1 v_i + o(h), \tag{39}$$

$$v_{i+1} + v_{i-1} = 2(D_1 v_i + D_2 v_i^{(1)}) + o(h^2), \tag{40}$$

$$v_{i+1} + v_{i-1} = 2(D_1 v_i + D_2 v_i^{(1)} + D_{31} v_i) + o(h^3). \tag{41}$$

To get the new finite difference schemes of the boundary condition (22), we begin with the formula:

$$v_{i+1} - v_{i-1} = 2\Big[\frac{h}{1!}v_i^{(1)} + \frac{h^3}{3!}v_i^{(3)} + \frac{h^5}{5!}v_i^{(5)} + \cdots + \frac{h^{2s-1}}{(2s-1)!}v_i^{(2s-1)} + \cdots\Big]. \tag{42}$$

Similarly, taking account of the contribution of all odd-order derivative terms by the original Helmholtz equation (20), it is easily known that all the terms of odd-order derivatives $v_i^{(2s-1)}(s = 1, 2, 3, \cdots)$ are only determined by $v_i, v_i^{(1)}$. Thus, (42) was rewritten as

$$v_{i+1} - v_{i-1} = 2[B_1 v_i^{(1)} + B_2 v_i + B_{31} v_i^{(1)} + \cdots]. \tag{43}$$

There hold that

$$\|B_1 v_i^{(1)}\| = O(h),\ \|B_2 v_i\| = O(h^2),\ \|B_{31} v_i^{(1)}\| = O(h^3),$$

where

$$B_1 = \frac{\sin(k_i h)}{k_i}, \tag{44}$$

$$B_2 = \frac{[-\frac{1}{4}k_i^2 h^2 \sin(k_i h) - \frac{1}{4}k_i h \cos(k_i h) + \frac{1}{4}\sin(k_i h)](k_i^2)^{(1)}}{k_i^3}, \tag{45}$$

$$B_{31} = \frac{[\frac{1}{12}k_i^3 h^3 \cos(k_i h) - \frac{1}{8}k_i^2 h^2 \sin(k_i h) - \frac{1}{8}k_i h \cos(k_i h) + \frac{1}{8}\sin(k_i h)](k_i^2)^{(2)}}{k_i^5}. \tag{46}$$

And the relationship for the boundary points are given:

$$v_{i+1} - v_{i-1} = 2B_1 v_i^{(1)} + o(h), \tag{47}$$

$$v_{i+1} - v_{i-1} = 2(B_1 v_i^{(1)} + B_2 v_i) + o(h^2), \tag{48}$$

$$v_{i+1} - v_{i-1} = 2(B_1 v_i^{(1)} + B_2 v_i + B_{31} v_i^{(1)}) + o(h^3). \tag{49}$$

Let V_i denote the approximation solution of v_i for the equation (20)–(22), following the analysis above, we get the following algorithms with the convergence order $O(h^t)$, where $t = 1, 2,$ and 3 respectively.

Algorithm 1

$$\begin{aligned} &-V_{i+1} - V_{i-1} + 2D_1 V_i = 0,\ 0 < i \le P,\\ &V_i = a^{\frac{1}{2}} g_1,\ i = 0,\\ &V_{i+1} - V_{i-1} - 2B_1(ik_n + \frac{1}{2r_i})V_i = 2B_1 b^{\frac{1}{2}} g_2,\ i = P. \end{aligned} \tag{50}$$

Algorithm 2

$$
\begin{aligned}
&-V_{i+1}-V_{i-1}+2D_1V_i+D_2\frac{V_{i+1}-V_{i-1}-2B_2V_i}{B_1}=0,\ 0<i\le P,\\
&V_i=a^{\frac{1}{2}}g_1,\ i=0,\\
&V_{i+1}-V_{i-1}-2[B_1+B_2(ik_n+\frac{1}{2r_i})]V_i=2B_1b^{\frac{1}{2}}g_2,\ i=P.
\end{aligned}\tag{51}
$$

Algorithm 3*

$$
\begin{aligned}
&-V_{i+1}-V_{i-1}+2(D_1+D_{31})V_i+D_2\frac{V_{i+1}-V_{i-1}-2B_2V_i}{(B_1+B_{31})}=0,\ 0<i\le P,\\
&V_i=a^{\frac{1}{2}}g_1,\ i=0,\\
&V_{i+1}-V_{i-1}-2[B_2+(B_1+B_{31})(ik_n+\frac{1}{2r_i})]V_i=2(B_1+B_{31})b^{\frac{1}{2}}g_2,\ i=P.
\end{aligned}\tag{52}
$$

Remark 3.1. *It was pointed out in* [30] *that Algorithms have the convergent order* $O(h^t)$ *with* $t=1,2,3$, *respectively, for problems in 2D and 3D. But for some cases in 1D, the convergence order of Algorithms 1, 2, and 3* could be higher.*

Next, we will deduce a more accurate scheme to solve the problem. Recall that [30],

$$
\begin{aligned}
\frac{h^{2n}}{(2n)!}&=O(h^{2n}),\ n=1,2\cdots,\\
\|v_i^{(n)}\|&=O(k^{n-1}),\ n=0,1,2,\\
\|(k_i^2)^{(n)}\|&=O(k^2),\ n\in Z,
\end{aligned}\tag{53}
$$

and

$$
v_i^{(2n)}=(v_i^{(2)})^{(2n-2)},\ v_i^{(2n-1)}=(v_i^{(2)})^{(2n-3)},\ n=1,2,3,\cdots.\tag{54}
$$

Thanks to (53) and (54), we can be recursive to know that all terms of derivatives $v_i^{(2n)}(n=1,2,3,\cdots)$ in (34) are only determined by $v_i, v_i^{(1)}$. There holds

$$
\begin{aligned}
\|\frac{h^{2n}}{2n!}v_i^{(2n)}\|&=\|\frac{h^{2n}}{2n!}(v^{(2)})^{(2n-2)}\|=\|\frac{h^{2n}}{2n!}(-k_i^2v_i)^{(2n-2)}\|\\
&=\|-\frac{h^{2n}}{2n!}[\sum_{m=0}^{2n-2}C_{2n-2}^m(k_i^2)^{(2n-2-m)}v_i^{(m)}]\|\\
&=O(h)+O(h^2)+O(h^3)+\cdots+O(h^{2n-1}).
\end{aligned}\tag{55}
$$

If we go back to the Algorithm 3*, there are not only terms respect to $(k_i^2)^{(2)}v_i$ equivalent to $O(h^3)$, but also terms related to $[(k_i^2)^{(1)}]^2v_i$ equivalent to $O(h^3)$ on the right hand side term of (34). Now, we will consider a correction of Algorithm 3* which is called Algorithm 3. Since more information is included in Algorithm 3 compared to Algorithm 3*, it is obtained that the former is more robust than the latter. The detail is as follows. To consider the terms equivalent to $O(h^3)$ included in $\frac{h^{2n}}{(2n)!}v_i^{(2n)}, n=2,3,\cdots$, we only need to consider the terms equivalent to $O(k^{2n-3}), n=2,3,\cdots$ in $v_i^{(2n)}$. For instance, when $n=3$, to consider terms equivalent to $O(h^3)$ included in $\frac{h^6}{6!}v_i^{(6)}$, we need to take account of the terms of $O(k)$ related to $[(k_i^2)^{(1)}]^2v_i$ in $v_i^{(6)}$, that is

$$
v_i^{(6)}\to O(k^3)\sim(-k_i^2v_i)^{(4)}\to O(k^3),\tag{56}
$$

there are three terms equivalent to $O(k^3)$

$$(57)\quad \begin{cases} -C_4^4 k_i^2 v_i^{(4)} \to O(k^3) \sim v_i^{(4)} \to O(k) \sim (-C_2^0 (k_i^2)^{(2)} v_i) \to O(k), \\ -C_4^3 (k_i^2)^{(1)} v_i^{(3)} \to O(k^3) \sim v_i^{(3)} \to O(k) \sim (-C_1^0 (k_i^2)^{(1)} v_i) \to O(k), \\ -C_4^2 (k_i^2)^{(2)} v_i^{(2)} \to O(k^3) \sim v_i^{(2)} \to O(k), \end{cases}$$

which yields

$$(58)\quad \frac{h^6}{6!}[C_4^4 k_i^2 C_2^0 (k_i^2)^{(2)} v_i + C_4^2 (k_i^2)^{(2)} (k_i^2) v_i] = \frac{h^6 k_i^2}{6!}(C_2^0 + C_4^2)(k_i^2)^{(2)} v_i = O(h^3),$$

$$(59)\quad \frac{h^6}{6!}(-C_4^3 (k_i^2)^{(1)})(-C_1^0 (k_i^2)^{(1)} v_i) = (-1)^2 \frac{h^6 k_i^2}{6!} C_4^3 C_1^0 ((k_i^2)^{(1)})^2 v_i = O(h^3).$$

Since (58) is included in Algorithm 3*, we only need to collect the contribution of (59).

Generally, the terms equivalent to $O(h^3)$ in $\frac{h^{2n}}{(2n)!} v_i^{(2n)}$ related to $[(k_i^2)^{(1)}]^2 v_i$ are as follows

(60)

$$(-1)^{n-1} \frac{h^{2n} k_i^{2n-6}}{2n!}[C_4^3 + C_6^5(1 + C_3^2) + \cdots + C_{2n-2}^{2n-3} \sum_{m=3}^{n} C_{2m-5}^{2m-6}][(k_i^2)^{(1)}]^2 v_i = O(h^3).$$

Collecting the contribution of all terms on the right hand side in (34) related to $[(k_i^2)^{(1)}]^2 v_i$ which are equivalent to $O(h^3)$, we have

$$D_{32} := \{\frac{k_i^2 h^6}{6!} C_4^3 - \frac{k_i^4 h^8}{8!}[C_4^3 + C_6^5(1 + C_4^3)] + \cdots$$
$$+ (-1)^{n-1} \frac{k_i^{2n-6} h^{2n}}{(2n)!}[C_4^3 + C_6^5(1 + C_4^3) + \cdots + C_{2n-2}^{2n-3} \sum_{m=3}^{n} C_{2m-5}^{2m-6}] + \cdots\}[(k_i^2)^{(1)}]^2,$$

which can be rewritten as

$$(61)\quad \begin{aligned} D_{32} =& \frac{1}{k_i^6}[-\frac{1}{32} k_i^4 h^4 \cos(k_i h) + \frac{5}{48} k_i^3 h^3 \sin(k_i h) \\ &+ \frac{7}{32} k_i^2 h^2 \cos(k_i h) - \frac{7}{32} k_i h \sin(k_i h)][(k_i^2)^{(1)}]^2. \end{aligned}$$

Defining $D_3 := D_{31} + D_{32}$, there holds that

$$(62)\quad \|D_3 v_i\| = \|(D_{31} + D_{32}) v_i\| = O(h^3),$$

and a higher accurate new finite difference scheme is given by

$$(63)\quad v_{i+1} + v_{i-1} = 2[D_1 v_i + D_2 v_i^{(1)} + D_3 v_i] + O(h^4).$$

For the boundary point scheme, similarly, for equation (42), it can be derived that

$$(64)\quad v_{i+1} - v_{i-1} = 2[B_1 v_i^{(1)} + B_2 v_i + B_3 v_i^{(1)}] + O(h^4),$$

where

$$(65)\quad \begin{aligned} B_3 =& B_{31} + B_{32}, \\ B_{32} =& \frac{1}{k_i^7}[-\frac{1}{32} k_i^4 h^4 \sin(k_i h) - \frac{5}{48} k_i^3 h^3 \cos(k_i h) + \frac{5}{32} k_i^2 h^2 \sin(k_i h) \\ &+ \frac{5}{32} k_i h \cos(k_i h) - \frac{5}{32} \sin(k_i h)][(k_i^2)^{(1)}]^2, \end{aligned}$$

and there holds that

$$(66)\quad \|B_3 v_i^{(1)}\| = \|(B_{31} + B_{32}) v_i^{(1)}\| = O(h^3).$$

Therefore, we have the new scheme

Algorithm 3

$$
\begin{aligned}
&V_{i+1}+V_{i-1}-2(D_1+D_3)V_i-D_2\frac{V_{i+1}-V_{i-1}-2B_2V_i}{(B_1+B_3)}=0,\ 0<i<N,\\
&V_i=a^{\frac{1}{2}}g_1,\ i=0, \qquad (67)\\
&V_{i+1}-V_{i-1}-2[B_2+(B_1+B_3)(jk+\frac{1}{2r_i})]V_i=2(B_1+B_3)b^{\frac{1}{2}}g_2,\ i=N.
\end{aligned}
$$

Wang et al. [30] have mentioned that if algorithms have the convergence orders $O(h^t)$, in practical computations, convergence order of algorithms could be one order higher for higher regularities of the solution are required when analyzing the finite difference scheme. Thus, it indicates that Algorithms 3 has the convergence orders $O(h^t)$ with $t = 4$.

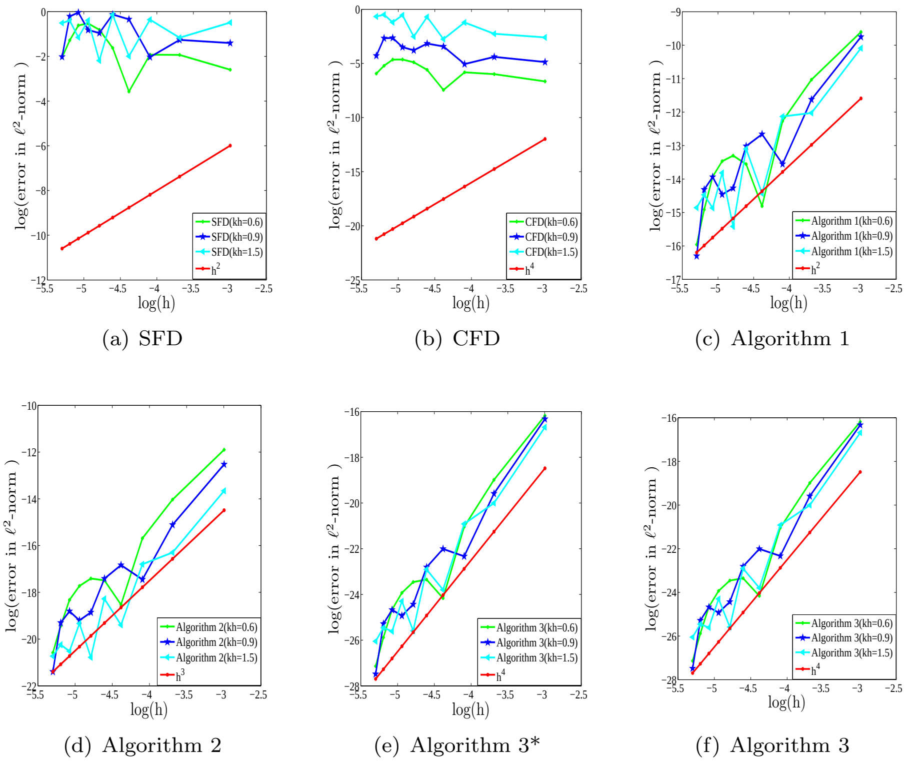

(a) SFD (b) CFD (c) Algorithm 1

(d) Algorithm 2 (e) Algorithm 3* (f) Algorithm 3

FIGURE 1. Convergence order of the different schemes with $kh = 0.6, 0.9, 1.5$ for Problem 1.

4. Numerical examples

In this section, we will show some numerical examples to verify the efficiency of the new schemes for the Helmholtz equation in the circular cylindrical coordinate. The numerical environment is characterized by the following parameters: the waveguide depth $H = 4$, the radius of the circular cylindrical obstacles Ω_1 $a = 1$, the radius of exterior boundary of Ω_2 $b = 2$, the source is located at depth $z_0 = \frac{H}{2}$, with the moving direction $\theta' = \frac{\pi}{4}$, and the source to the border of the circular cylindrical obstacles distance is 1.5.

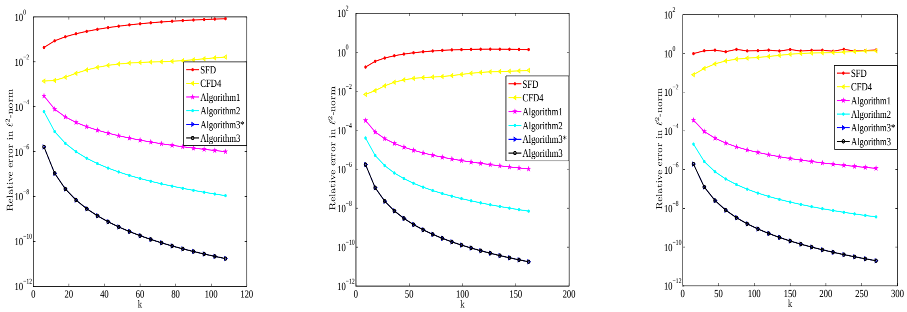

(a) $kh = 0.6$ (b) $kh = 0.9$ (c) $kh = 1.5$

FIGURE 2. Relative error in ℓ^2-norm with respect to k with $kh = 0.6, 0.9, 1.5$ for Problem 1.

Problem 1. *Performance in 1D*

Firstly, setting the exact solution,

$$u^s_{mn} = c_{mn} H^{(1)}_m(k_n r),$$

we verify the convergence order and the development of the relative error in ℓ^2-norm of the 1D problem (16)–(18). For simplicity, we let $n = 1, m = 1$. But in such case, Algorithms 1-3 have the convergence orders $O(h^t)$ with $t = 2, 3$ and 4, respectively (see Remark 4.1). In Fig. 1, we can see that, compared with the SFD and CFD schemes, the convergence order of new finite difference schemes can keep highly stable when $kh = 0.6, 0.9$ and 1.5. With the assumption kh being a constant, the wave number k will increase as the mesh size h decreases. Based on this observation, further illustrations are shown in Fig. 2, we find that the relative errors of Algorithms 1-3 decrease as the wave number k increases, the higher order the algorithm has, the less relative error it gets, while the relative error of the SFD and CFD schemes will increase as the wave number k is increasing. And it seems that Algorithms 3 have the same relative error as Algorithms 3*, but in fact, the relative error of Algorithms 3 is smaller than Algorithms 3*, especially for 2D problem (see Fig. 4). Dramatically show the new finite difference schemes are "pollution free", what's more, the wave number k is even larger more than 96.

Remark 4.1. *With the exact solution in Problem 1, g_{2mn} in* (18) *is $O(k)$ which does not satisfy the assumption in Lemma 2.1. But the following stability results can be obtained by a similar process:*

$$\begin{aligned} \| u^s_{mn} \| &= O(1), \\ \| {u^s_{mn}}^{(1)} \| &= O(k), \\ \| {u^s_{mn}}^{(2)} \| &= O(k^2). \end{aligned}$$

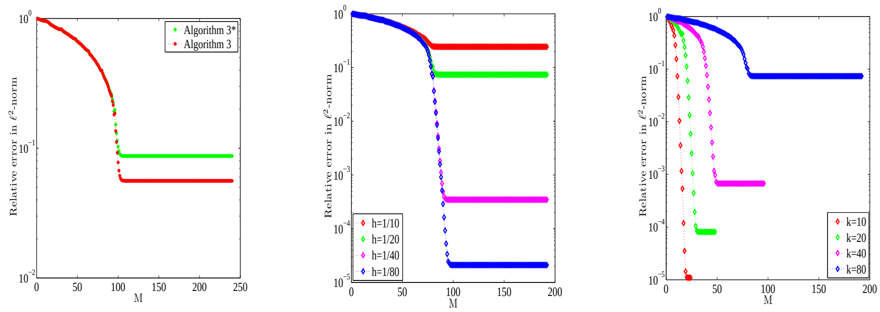

(a) $k = 100, a = 1, b = 2$ (b) $k = 80, a = 1, b = 2$ (c) $h = 0.05, a = 1, b = 2$

FIGURE 3. Relative error in ℓ^2-norm with respect to M for Problem 2 of Algorithm 3.

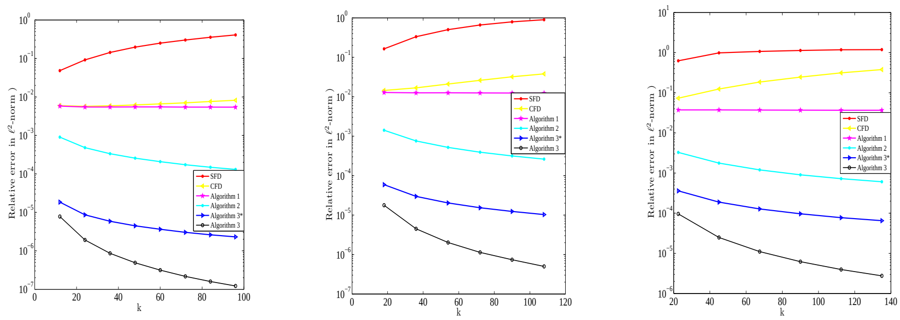

(a) $kh = 0.6$ (b) $kh = 0.9$ (c) $kh = 1.5$

FIGURE 4. Relative error in ℓ^2-norm with respect to k with $kh = 0.6, 0.9, 1.5$ for Problem 2.

Since in this case $k^s_{mn} = k^2 - ((1+\frac{1}{2})\frac{\pi}{H}) - \frac{1}{r^2}$, (27) *could be reduced to* $\|k^2(r)\| = O(k^2)$, *and* $\|k^2(r)^{(l)}\| = O(1), l \in Z^+$. *According to the derivation of Algorithms 1, 2, 3** [30] *and 3, the terms* $D_1 v_i, D_2 v_i^{(1)}, D_3 v_i$, *will satisfy*

$$\|D_1 v_i\| = O(h^2),$$
$$\|D_2 v_i^{(1)}\| = O(h^3),$$
$$\|D_3 v_i\| = O(h^4),$$

So the convergence order of new finite difference schemes, Algorithms 1, 2, 3 and 3, will be one-order higher than that claimed in the above section.*

Problem 2. *Acoustic scattering from a circular cylindrical obstacle*

As described in Section 2, the acoustic scattering from the circular cylindrical obstacle in a 3D ocean shallow waveguide can be presented as follows:

$$u^s = \sum_{n=0}^{N-1} \sum_{m=-\infty}^{+\infty} u^s_{mn}(r)\psi_m(\theta)\omega_n(z), \text{ in } \Omega_2 \backslash \Omega_1.$$

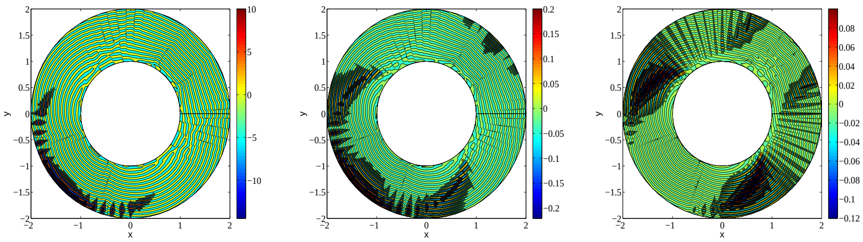

(a) SFD (b) CFD (c) Algorithm 1

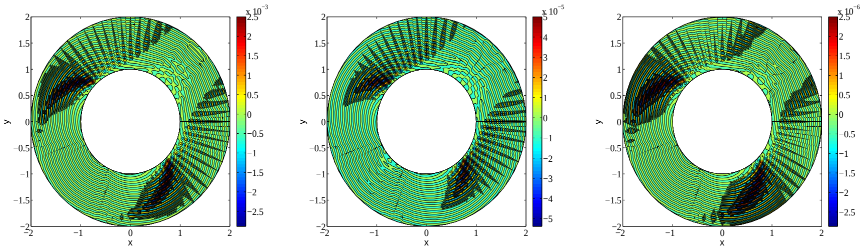

(d) Algorithm 2 (e) Algorithm 3* (f) Algorithm 3

FIGURE 5. The error in the horizontal direction with $kh = 0.6, k = 96, z = 2$ for Problem 2.

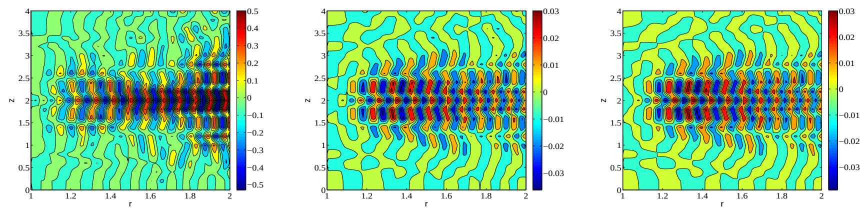

(a) SFD (b) CFD (c) Algorithm 1

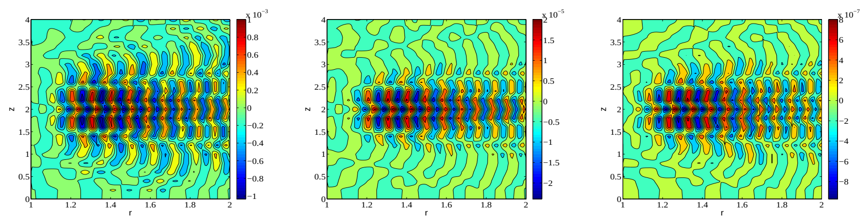

(d) Algorithm 2 (e) Algorithm 3* (f) Algorithm 3

FIGURE 6. The error in the vertical direction with $kh = 0.6, k = 96, \theta = \frac{\pi}{2}$ for Problem 2.

Using Algorithm 3, we first test the convergence of the series with respect to M in the above representation. Fig. 3 (a), for a fixed wave number $k = 100$, shows that Algorithm 3 is more accurate than Algorithm 3*, since Algorithm 3 is a correction

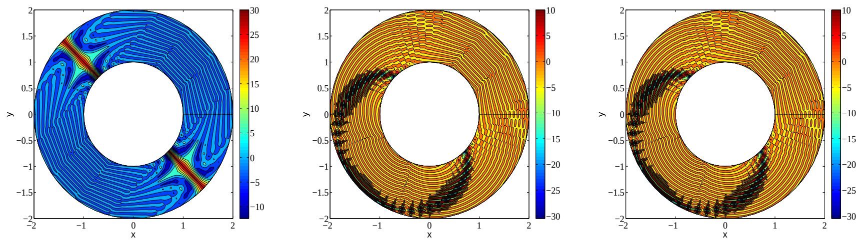

(a) Incident wave (b) Exact solution (c) Algorithm 3

FIGURE 7. The real part of the incident wave, exact solution, numerical solution with $kh = 0.6, k = 96, z = 2$ for Problem 2.

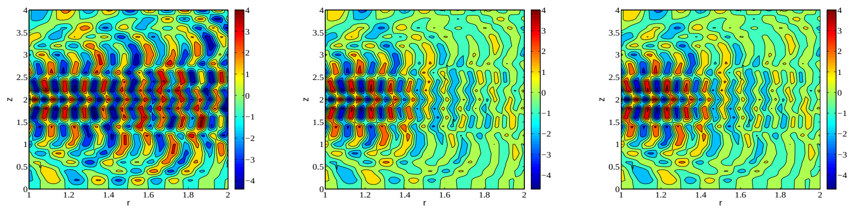

(a) Incident wave (b) Exact solution (c) Algorithm 3

FIGURE 8. The real part of the incident wave, exact solution, numerical solution with $kh = 0.6, k = 96, \theta = \frac{\pi}{2}$ for Problem 2.

of Algorithm 3*. Fig. 3 (b), for a fixed wave number $k = 80$, shows that the convergence of the summation in the above equation almost depends on the same M with different mesh sizes. While for a fixed mesh size $h = 0.05$, Fig. 3 (c) shows that the convergence depends on different M with different wave number k, and that the value of M increases when the wave number k increases, which is in agreement with the result in [15]. Further investigation is presented in Fig. 4. It is apparent that the new finite difference schemes are "pollution free" and the wave number k is greater than that in the literatures (see [3, 20]). On the other hand, in studying wave propagation problems numerically, the following "rule of thumb" is necessary:

$$PPW := \frac{\lambda}{h} = \frac{2\pi}{kh},$$

where PPW implies the discretization point per wavelength, $\lambda = \frac{2\pi}{k}$ is the wave length. It's well known that, for the simulation of the waveguide problem that $PPW = 10$ ensures reliable results, and this leads $kh \approx 0.6$. So we just consider the condition $kh \approx 0.6$. Setting $error = u^s - U^s$, where $U^s = \{U_i^s\}_{i=0}^P = \{r_i^{-\frac{1}{2}} V_i\}_{i=0}^P$ is the numerical solution. Fig. 5 and 6 show the error from the horizontal direction and vertical direction, respectively. It is apparently indicated by there results that more accurate approximation solutions can be obtained by applying new Algorithms 1, 2, 3* and 3, especially Algorithm 3. The accuracy in horizontal reach 10^{-6} and vertical direction reach 10^{-7} for Algorithm 3, while the CFD method just obtains 10^{-2} in the vertical direction and 10^{-1} in the horizontal direction. We observe worse results for the SFD, and the reason is that in the horizontal direction, all truncation errors are determined by k^3h^2, and the approximation accuracy depends essentially on the wave number k. Finally, with the incident wave as mentioned above, we simulate the actual physical features in the horizontal and vertical direction using Algorithm 3, and the contour graphs are shown in Figs. 7-8 when $kh = 0.6$ with $k = 96$. Fig. 7 shows the results in the horizontal direction with $z = 2$, and Fig. 8 shows the results in the vertical direction with $\theta = \frac{\pi}{2}$. It turns out that the new finite difference scheme has the feature of high resolution.

5. Conclusions

In this paper, using the new finite difference schemes proposed in [30], and constructing a more accurate finite difference scheme, we considered the 3D acoustic scattering by an impenetrable cylindrical obstacle in shallow ocean. We verify the efficiency of the new finite difference scheme. Numerical results demonstrate that the new finite difference schemes are efficient for some complicated cases, such as, horizontally stratified ocean waveguide penetrable obstacles and ellipse obstacles (see [19]).

References

[1] G.A. Athanassoulis, A.M. Prospathopoulos, Three-dimensional acoustic scattering of a source-generated field from a cylindrical island, J. Acoust. Soc. Am., 100 (1996) 206-218.

[2] G.A. Athanassoulis, K.A. Belibassakis, All-frequency normal-mode solution of the three-dimensional acoustic scattering from a vertical cylinder in a plane-horizontal waveguide, J. Acoust. Soc. Am., 101 (1997) 3371-3384.

[3] L. Bourgeois, C. Chambeyron, S. Kusiak, Locating an obstacle in a 3D finite depth ocean using the convex scattering support, J. Comput. Appl. Math., 204 (2007) 387-399.

[4] M.J. Buckingham, Ocean-acoustic propagating models, J. Acoust., 5 (1992) 223-287.

[5] J.L. Buchanan, R.P. Gilbert, A. Wirgin, Y.Z. Xu, Identification, by the intersecting canonical domain method, of the size, shape and depth of a soft body of revolution located within an acoustic waveguide, Inverse Problems, 16 (2000) 1709-1726.

[6] P.M.V.D. Berg, J.T. Fokkema, The Rayleigh hypothesis in the theory diffraction by a cylindrical obstacls, IEEE. Trans. Antennas and Propagation, 27 (1979) 577-583.

[7] D. Colton, R. Kress, Inverse Acoustic and Electromagnetic Scattering Theory, 2nd Edition, Springer-Verlag: Berlin, 1998.

[8] R.B. Evans, A coupled mode solution for acoustic propagation in a waveguide with stepwise depth variations of a penetrable bottom, J. Acoust. Soc. Am., 74 (1983) 188-195.

[9] J.A. Fawcett, An efficient three-dimensional boundary integral equation method for solving azimuthally symmetric scattering problems in the oceanic waveguide, J. Acoust. Soc. Am., 94 (1993) 2307-2314.

[10] J. Gracia, E. O$'$Riordan, Interior layers in a singularly perturbed time dependent convection-diffusion problem, Int. J. Numer. Anal. Model., 11 (2014) 358-371.

[11] C.H. Harrison, Ocean propagation models, Appl. Acoust., 27 (1989) 163-201.

[12] X. He, K. Wang, New finite difference methods for convection-diffusion equations with small singularly perturbed coefficients, submitted.

[13] G.C. Hsiao, N. Nigam, J.E. Pasciak, L. Xu, Error analysis of the DtN-FEM for the scattering problem in acoustics via Fourier analysis, J. Comput. Appl. Math., 235 (2011) 4949-4965.

[14] Q. Hu, L. Yuan, A weighted variational formulation based on plane wave basis for discretization of Helmholtz equations, Int. J. Numer. Anal. Model., 11 (2014) 587-607.

[15] F. Ihlenburg, Finite Element Analysis of Acoustic Scattering, Spring, NewYork, 1998.

[16] F. Jensen, Computational ocean acoustics: forward and inverse methods, in lecture notes of the Advanced Course on Acoustical Oceanography (Iraklion, Crete), (1993) 7-19.

[17] W. Luo, H. Schmidt, Three-dimensional propagation and scattering around a conical seamount, J. Acoust. Soc. Am., 125 (2009) 52-65.

[18] D. Lee, Ocean acoustic propagation by finite difference methods, Elsevier Ltd., 1988

[19] L. Ma, J. Shen, L. Wang, Spectral approximation of time-harmonic Maxwell equation in three-dimensional exterior domains, Int. J. Numer. Anal. Model., 12 (2015) 366-383.

[20] W.F. Pan, Y.X. You, G.P. Miao, Z.Q. Li, A coupled FE and DtN mapping method for the exterior problem of the Helmholtz Equation in an oceanic waveguide, ACTA Acustica united with Acustica, 94 (2008) 301-309.
[21] A. Peplowa, S. Finnveden, A super-spectral finite element method for sound transmission in waveguides, J. Acoust. Soc. Am., 116 (2004) 1389-1400.
[22] J.X. Qin, W.Y.R. Luo, H. Zhang, C.M. Yang, Numerical solution of range-dependent acoustic propagation, Chin. Phys. Lett., 30 (2013) 0743011-0743014.
[23] J.X. Qin, W.Y.R. Luo, H. Zhang, C.M. Yang, Three-dimensional sound propagation and scattering in two-dimensional waveguides, Chin. Phys. Lett., 30 (2013) 1143011-1143014.
[24] J. Shen, L. Wang, Spectral approximation of the Helmholtz equation with high wave numbers, SIAM J. Numer. Anal., 43 (2006) 623-644.
[25] M. Porter, E.L. Reiss, A numerical methods for ocean-acoustic normal modes, J. Acoust. Soc. Am., 76 (1984) 244-252.
[26] C.P. Vendhan, G.C. Diwan, Bhattacharyya, S. K., Finite-element modeling of depth and range dependent acoustic propagation in oceanic waveguides, J. Acoust. Soc. Am., 127 (2010) 3319-3327.
[27] Y.S. Wong, G. Li, Exact finite difference schemes for solving Helmholtz equation at any wavenumber, Int. J. Numer. Anal. Model. Ser. B, 2 (2011) 91-108.
[28] K. Wang, Y.S. Wong, Pollution-free finite difference schemes for non-homogeneous Helmholtz equation, Int. J. Numer. Anal. Model., 11 (2014) 787-815.
[29] K. Wang, Y.S. Wong, Is pollution effect of finite difference schemes avoidable for multi-dimensional Helmholtz equations with high wave numbers? Commun. Comput. Phys., accepted.
[30] K. Wang, Y.S. Wong, J. Deng, Efficient and accurate numerical solutions for Helmholtz equation in polar and spherical coordinates, Commun. Comput. Phys., 17 (2015) 779-807.
[31] T.W. Wu, On computational aspects of the boundary element method for acoustic radiation and scattering in a perfect waveguide, J. Acoust. Soc. Am., 96 (1994) 3733-3743.
[32] Y. Z. Xu, The propagating solutions and far-field patterns for acoustic harmonic waves in a finite depth ocean, Appl. Anal, 35 (2007) 129-151.
[33] Z. G. Yang, L.L. Wang, Accurate simulation of circular and elliptic cylindrical invisibility cloaks, Commun. Comput. Phys., 17 (2015) 822-849.
[34] W.S. Zhang, Y.Y. Dai, Finite-difference solution of the Helmholtz equation based on two domain decomposition algorithms, J. Appl. Math. Phy., 1 (2013) 18-24.
[35] S. Zhang, Z. Li, L. Wang, An-augumented IIM for Helmholtz/Possion equations on irregular domain in complex space, Int. J. Numer. Anal. Model., 13 (2016) 166-178.

[1] College of Mathematics and Statistics, Chongqing University, Chongqing 401331, P.R. China

[2] Institute of Computing and Data Sciences, Chongqing University, Chongqing 400044, P.R. China

[3] College of Sciences, Shihezi University, Xinjiang 832003, P.R. China
E-mail: guorui@shzu.edu.cn, kunwang@cqu.edu.cn and xul@cqu.edu.cn